Table S1. Overview of the observational time periods used for the trend analysis. We use the time period 2008–2022, which corresponds to rapid increases in CH_4 levels, whenever possible. CO columns inferred from IASI Metop-B are only available from 2014 onward and we also include 2023 in the trend analysis to improve the number of available data points for the linear fitting.

observation type	time period used for trend analysis
CSIRO surface flasks	2008-2022
NOAA surface flasks	2008-2022
HIPPO campaign	2009-2011
ATom campaign	2016-2018
IASI Metop-B satellite	2014-2023
MOPITT satellite	2008-2022

Table S2. Additional information on the airborne and surface measurement sites, which are used in this study.

site ID	observation type	data provider	calibration standard	latitude	longitude	altitude [m]
BHD	surface flask	NOAA	WMO X2025	41.41°S	174.87°E	92
CGO	surface flask	NOAA / CSIRO	WMO X2025 / CSIRO2020	40.68°S	144.68°E	160
CGO	surface in-situ	AGAGE	CSIRO2020	40.68°S	144.68°E	160
CPT	surface flask	NOAA	WMO X2025	34.35°S	18.49°E	260
CRZ	surface flask	NOAA	WMO X2025	46.43°S	51.85°E	202
DRP	shipboard flask	NOAA	WMO X2025	59.04°S	63.33°W	10
PSA	surface flask	NOAA	WMO X2025	64.77°S	64.05°W	15
SPO	surface flask	NOAA / CSIRO	WMO X2025 / CSIRO2020	89.98°S	24.80°W	2817
SYO	surface flask	NOAA	WMO X2025	69.00°S	39.58°E	17
USH	surface flask	NOAA	WMO X2025	54.85°S	68.31°W	32
CYA	surface flask	CSIRO	CSIRO2020	66.28°S	110.52°E	55
MAA	surface flask	CSIRO	CSIRO2020	67.62°S	62.87°E	40
MQA	surface flask	CSIRO	CSIRO2020	54.48°S	158.97°E	13
HIPPO	airborne in-situ	NASA/NOAA/NSF	WMO X2004	-	-	-
HIPPO	airborne flask	NOAA	WMO X2025	-	-	-
ATom	airborne in-situ	NASA/NOAA/NSF	WMO X2014A	-	-	-
ATom	airborne flask	NOAA	WMO X2025	-	-	-

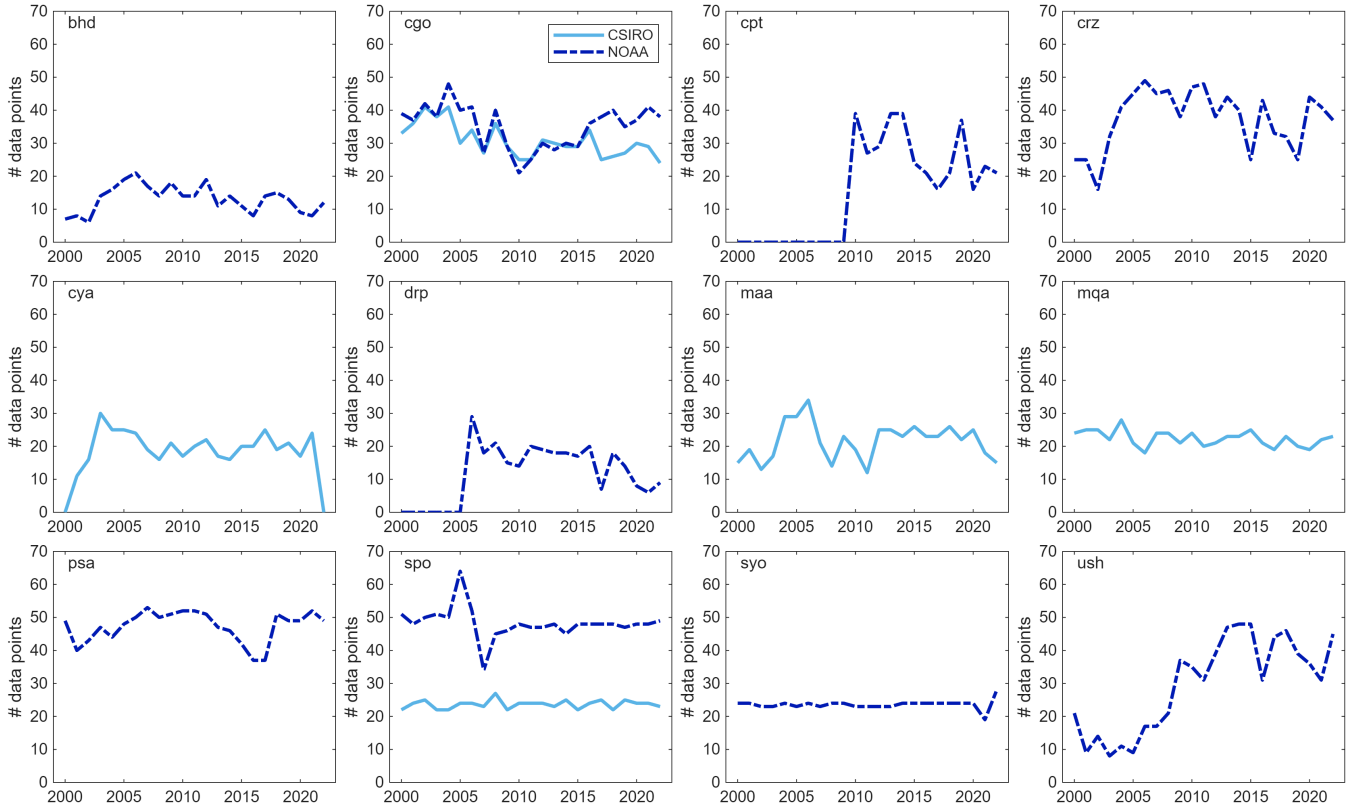

Figure S1. Overview of the number of data points at the individual surface flask sites included in the analysis. Light blue solid lines show numbers at the CSIRO sites and dark blue dashed lines represent the NOAA sites.

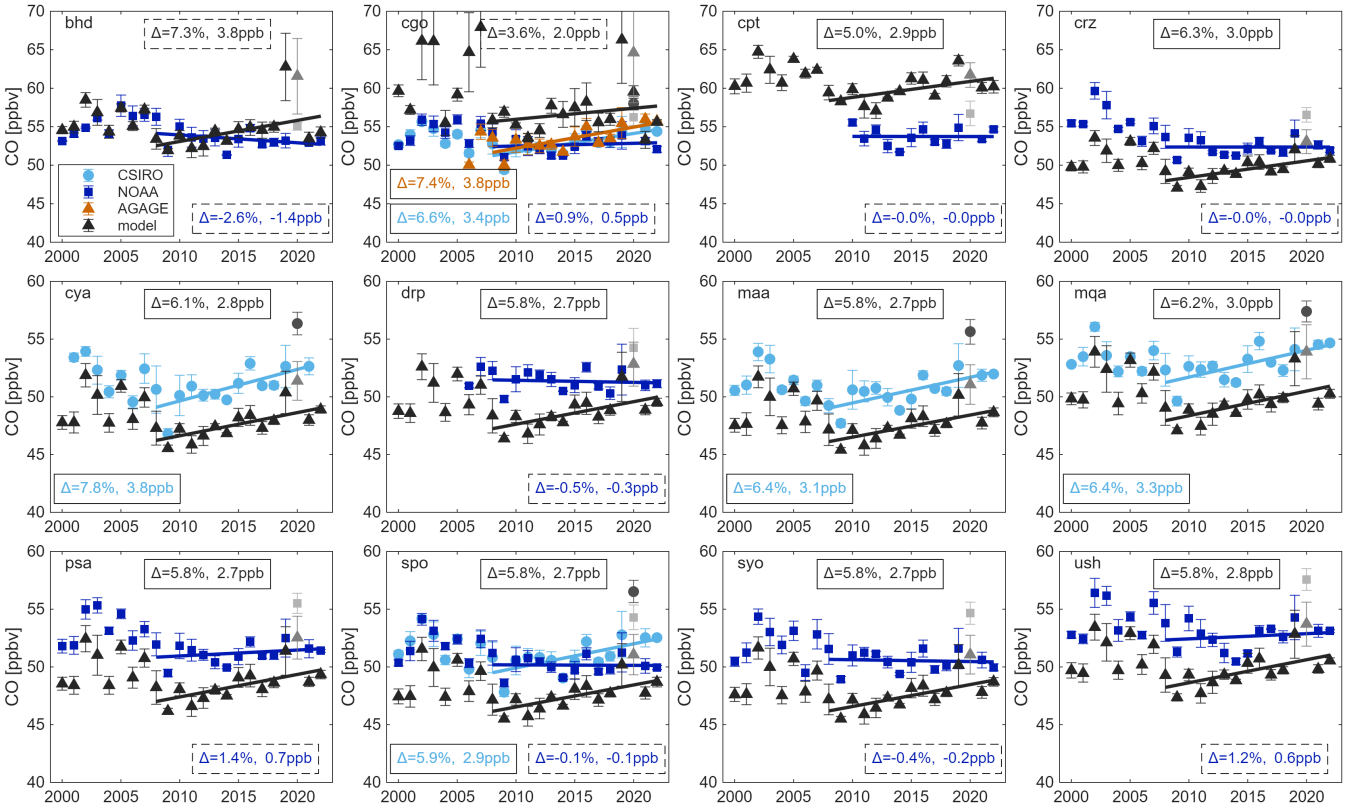

Figure S2. Observation-based and simulated CO between 2000 and 2022 at the individual surface flask sites. Annual means of CO at the CSIRO sites are shown in light blue, at the NOAA sites in dark blue and CO at the AGAGE site is represented in orange. Simulated CO is shown in gray. Symbols show yearly averages of the deseasonalized data (as described in the main text) and error bars highlight the uncertainty (root mean square value of the 1σ standard deviation from the yearly averaging of the deaseasonalized data at the individual sites). The lines indicate the linear fit between 2008 and 2022 and the boxes show the absolute and relative changes of CO over this time period. Solid boxes indicate significant (p-value$<$0.05) and dashed lines insignificant fits (p-value$>$0.05). We do not include the 2020 values (shown as open symbols) in the fit to avoid a high bias.

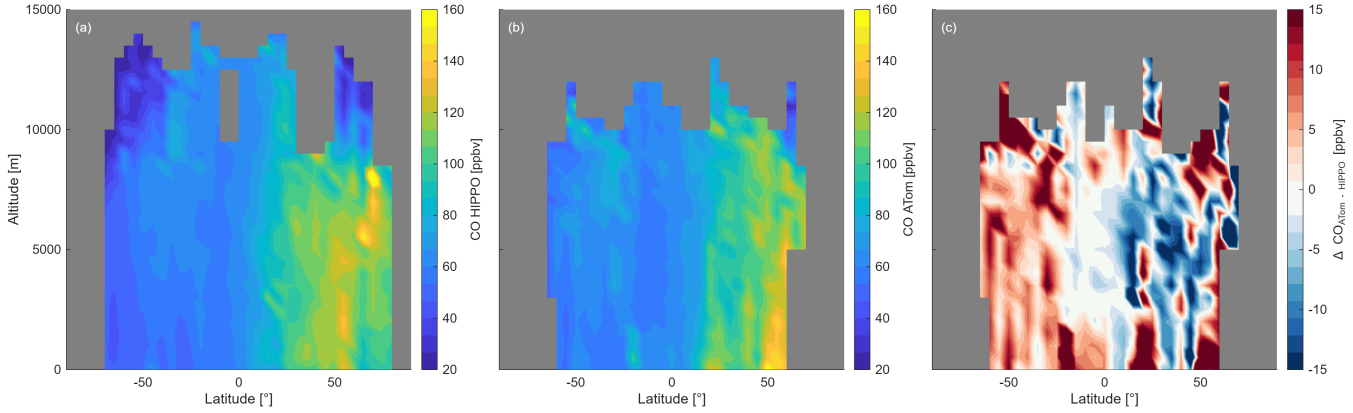

Figure S3. Zonal averages of observed CO **(a)** during the HIPPO campaigns (2009-11), **(b)** during the ATom campaigns (2016-18) and **(c)** the difference between ATom and HIPPO CO. Data were filtered for longitudes with availability of both ATom and HIPPO data: 180°W $\leq$ LON $\leq$ 150°W and 100°E $\leq$ LON $\leq$ 180°E.

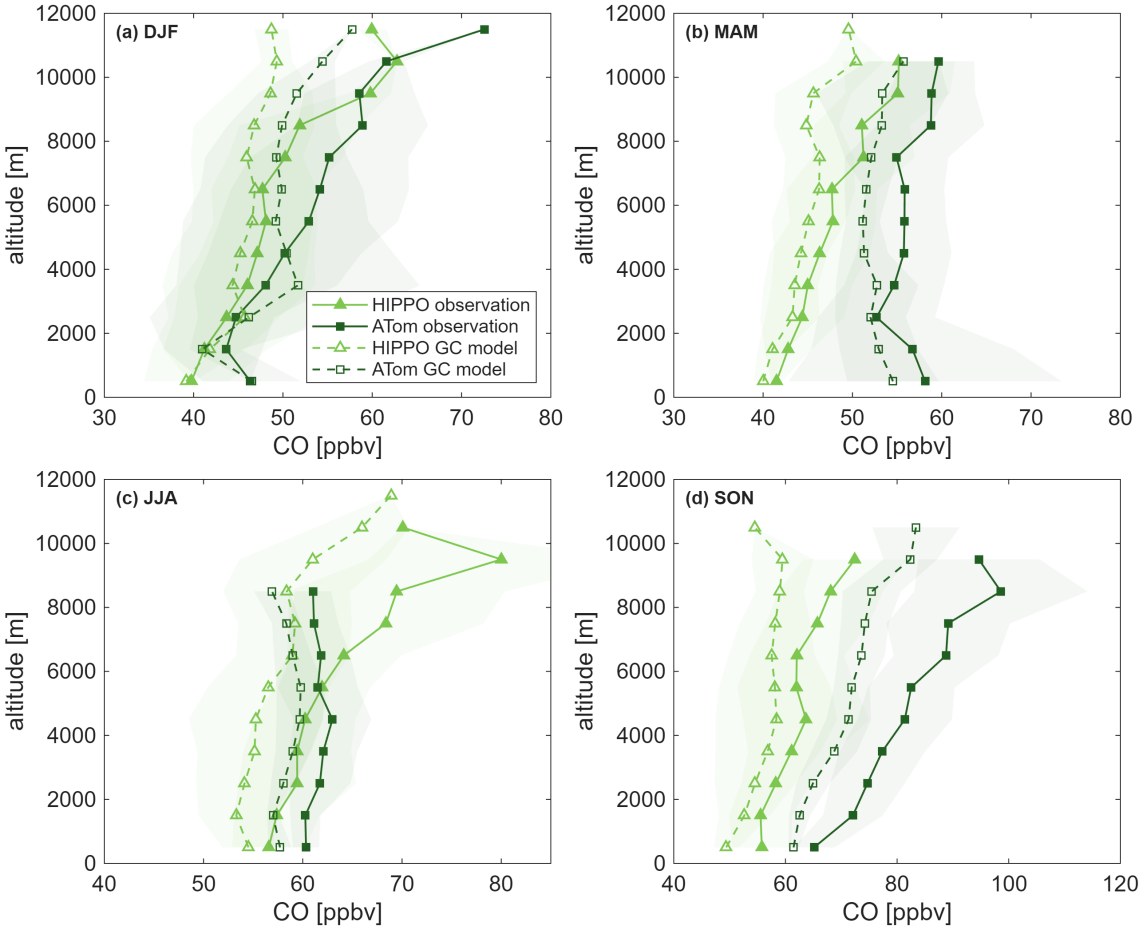

Figure S4. Mean vertical profiles of CO during the HIPPO (2009–2011, light green triangles) and the ATom campaigns (2016–2918, dark green squares), separated into individual seasons (DJF, MAM, JJA and SON). In-situ observations are shown by filled symbols and solid lines; GEOS-Chem (GC) simulated mixing ratios are presented by open symbols and dashed lines. Symbols represent averages binned to 1 km altitude and the shading indicates the 1σ standard deviation around the mean.

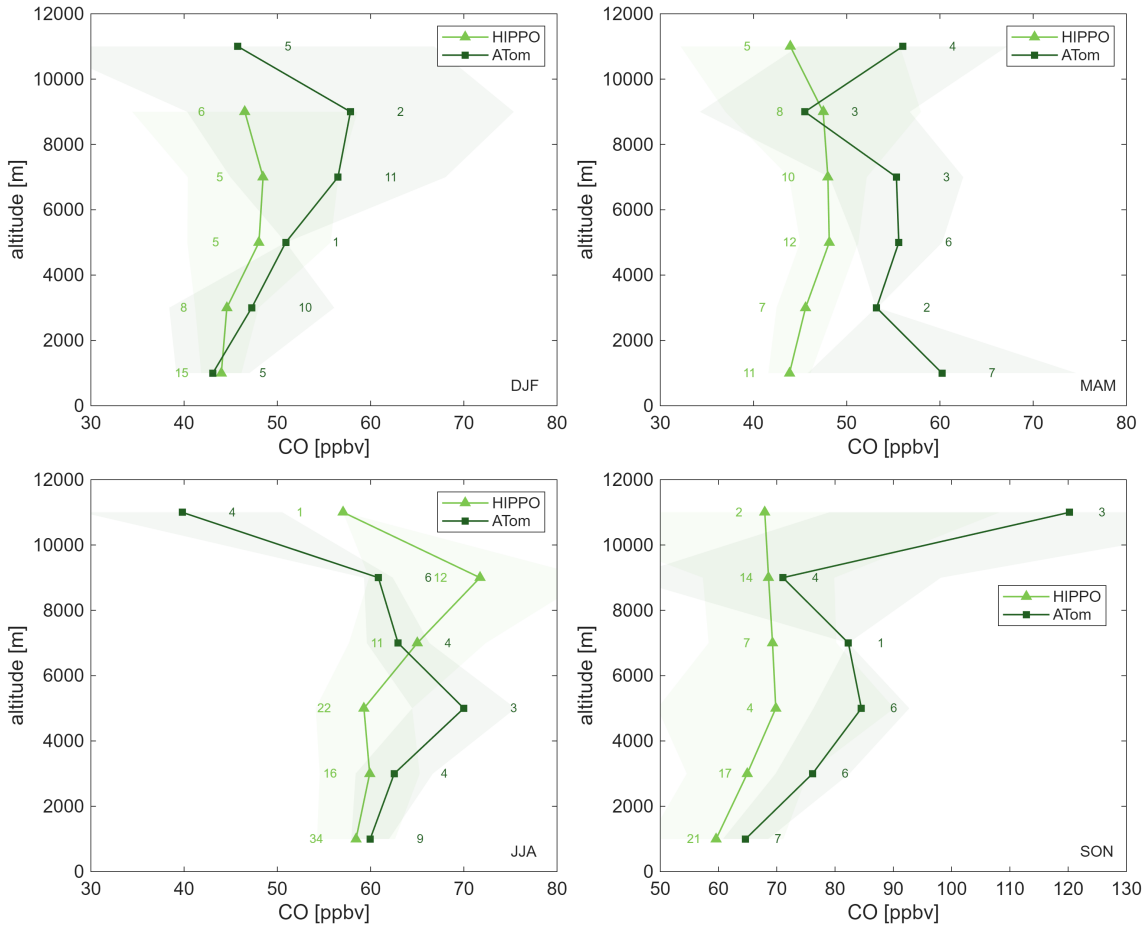

Figure S5. Mean vertical profiles of CO during the HIPPO (light green triangles) and the ATom campaigns (dark green squares) over the remote Southern Oceans based on Programmable Flask Package (PFP) data, separated into individual seasons (DJF, MAM, JJA and SON). Symbols represent averages binned to 2 km altitude and the shading indicates the 1σ standard deviation around the mean. The numbers indicate the available data points for each altitude bin.

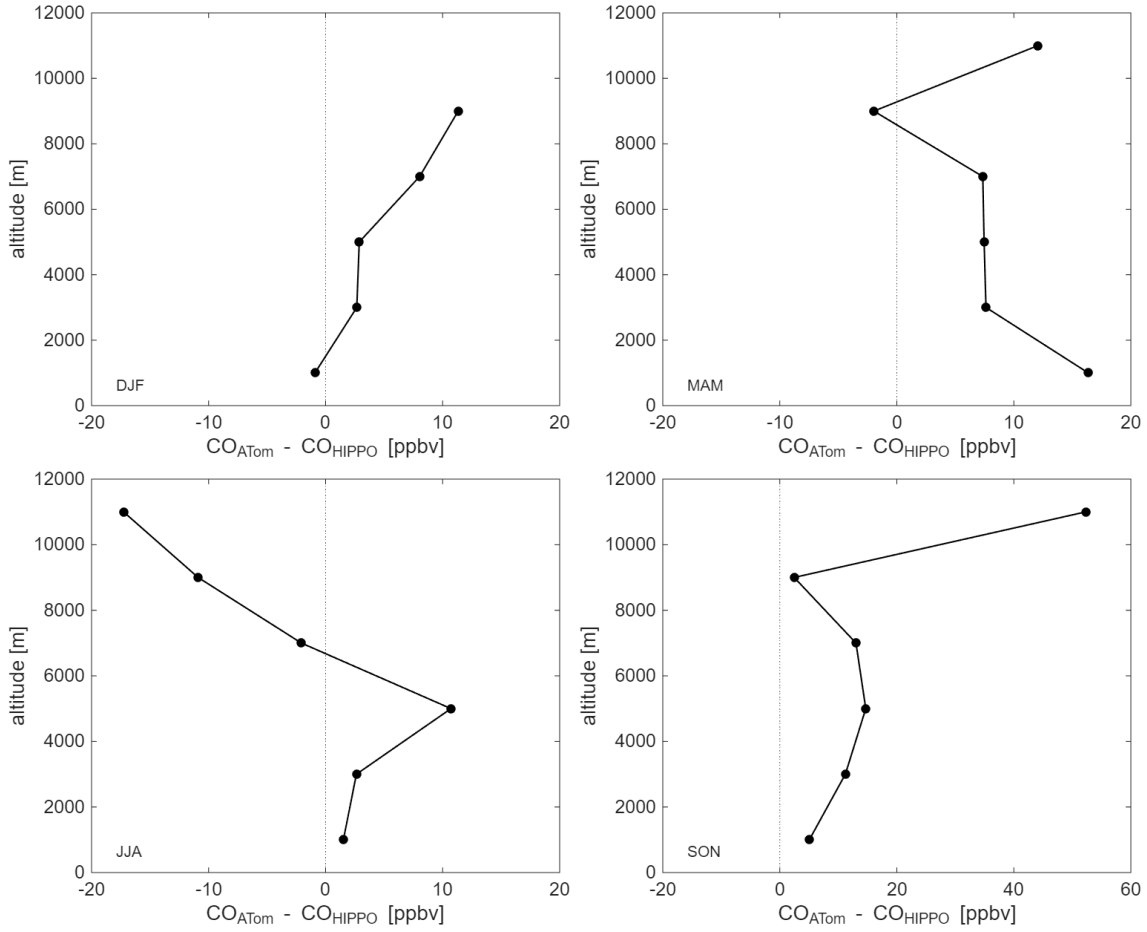

Figure S6. Difference in mean vertical profiles between ATom and HIPPO CO over the remote Southern Oceans based on Programmable Flask Package (PFP) data, separated into individual seasons (DJF, MAM, JJA and SON).

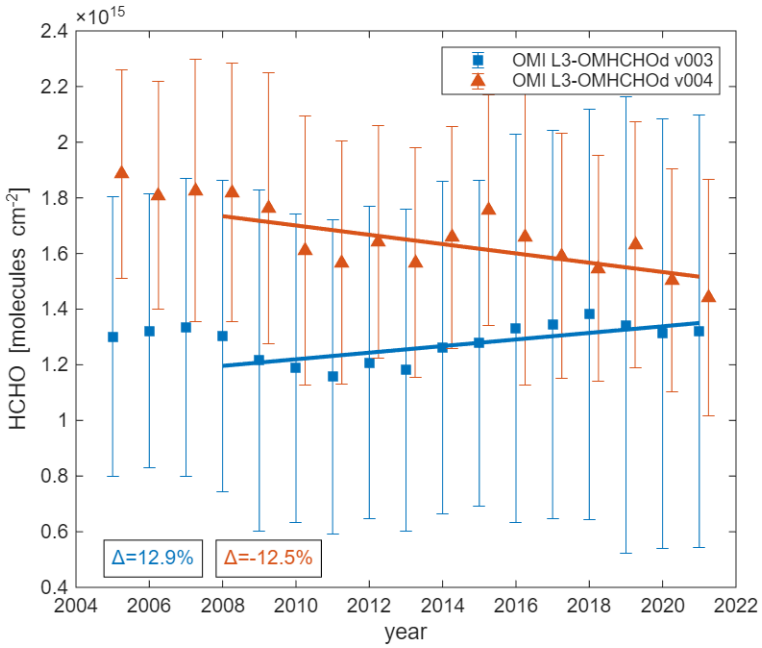

Figure S7. HCHO column changes between 2005 and 2021 based on satellite retrievals from the OMI instrument in version 3 (blue squares) and version 4 (orange triangles) South of 30°S. Symbols show yearly weighted averages (using the sample weight) and error bars represent the temporal uncertainty (1σ standard deviation of the temporal averaging). The solid lines indicate the linear fit between 2008 and 2021 and the boxes shows the relative change of HCHO over this time period. The trends are significant (p-value$<$0.05).

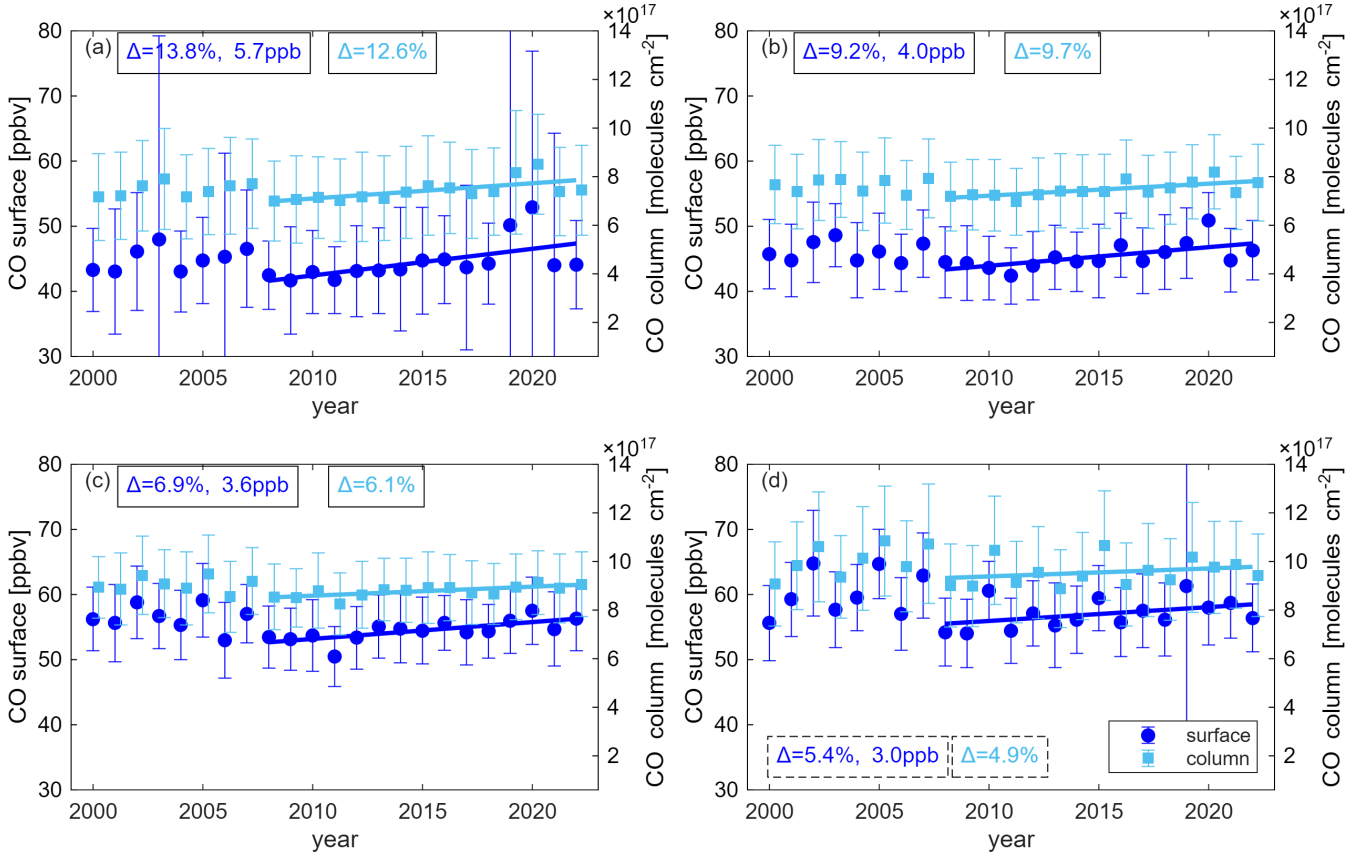

Figure S8. CO changes between 2000 and 2022 in the Southern Extratropics (LAT $< 30°$S) as simluated by GEOS-Chem for **(a)** DJF, **(b)** MAM, **(c)** JJA and **(d)** SON. Dark blue colors show mixing ratios ar the surface and light blue colors indicate columns throughout the troposphere. Circles and squares show yearly averages and error bars represent the 1σ standard deviation of the averaging. The solid lines indicate the linear fit between 2008 and 2022 and the boxes show the absolute and relative changes of CO over this time period. Solid boxes indicate significant (p-value$<$0.05) and dashed boxes insignificant trends (p-value$\geq$0.05).

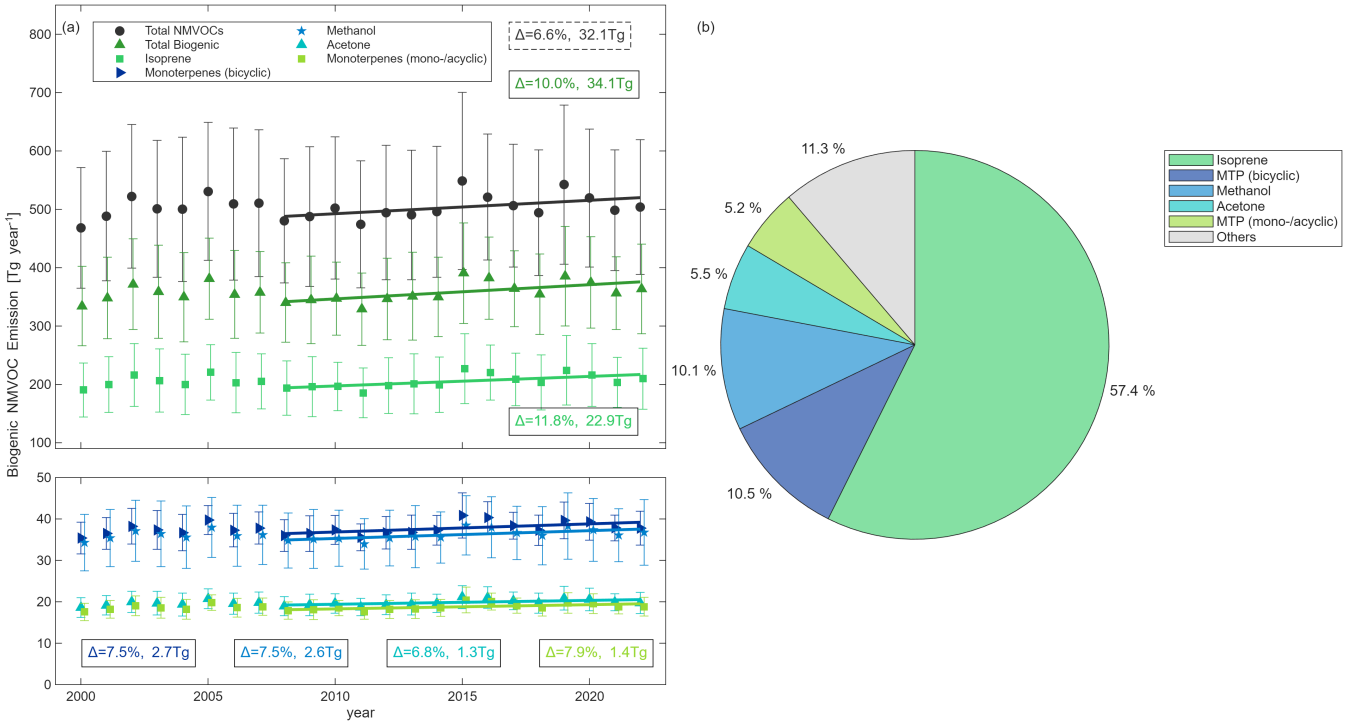

Figure S9. **(a)** Changes of biogenic NMVOC emissions in the SH between 2000 and 2022. Symbols show yearly averages and error bars represent the 1σ standard deviation of the averaging. The lines indicate the linear fit between 2008 and 2022 and the boxes show the changes over this time period. All fits are significant (p-value$<$0.05). **(b)** The share of individual NMVOC emissions in the total biogenic NMVOC emissions in the SH.

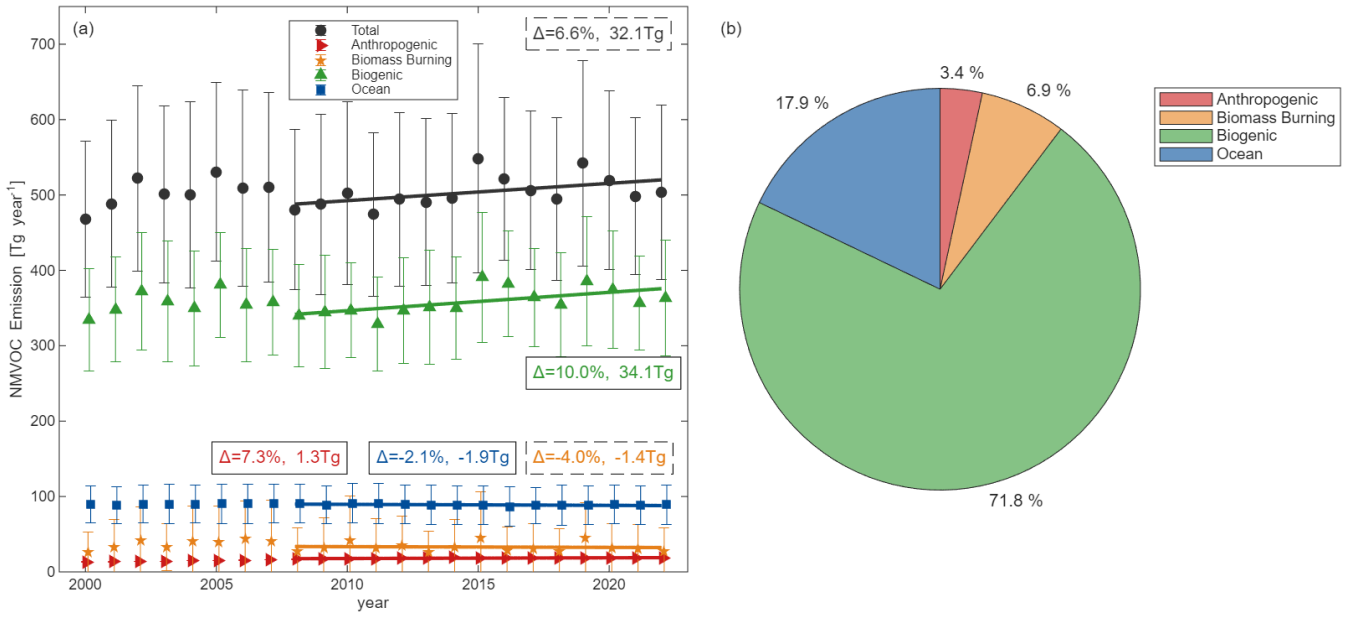

Figure S10. (a) Changes of NMVOC emissions from different sources as represented in GEOS-Chem. Symbols show yearly averages and error bars represent the 1σ standard deviation of the averaging. The solid lines indicate the linear fit between 2008 and 2022 and the boxes show the absolute and relative changes of CO over this time period. Solid boxes indicate significant (p-value$<$0.05) and dashed boxes insignificant trends (p-value$\geq$0.05). **(b)** The relative contribution of individual emission types to the overall NMVOC source.

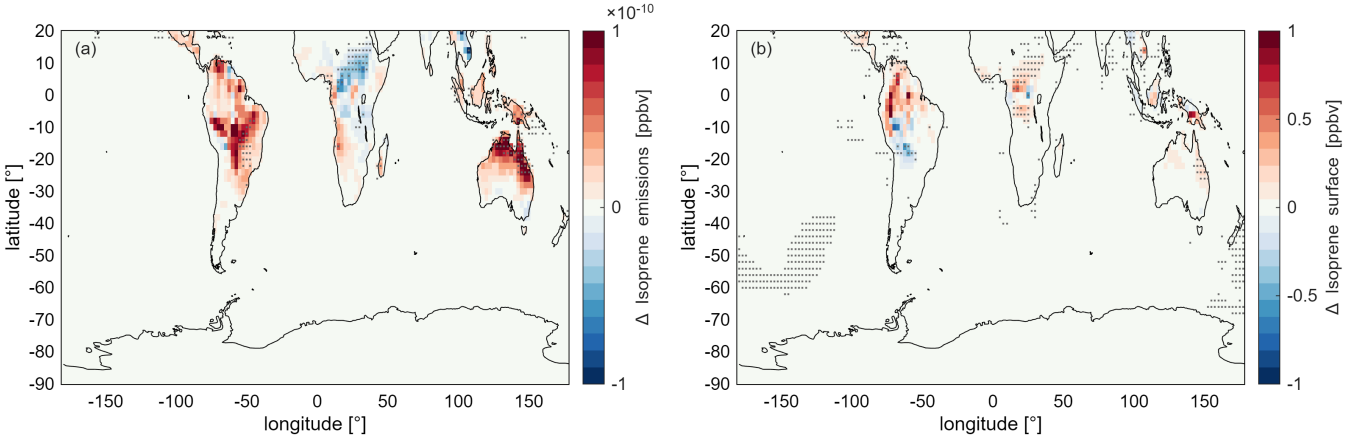

Figure S11. Simluated changes of **(a)** isoprene emissions and **(b)** surface isoprene between 2008 and 2022. Red colors show increases and blue colors decreases. Dots indicate significant changes (p-value$<$0.05) & $R^2>0.3$).

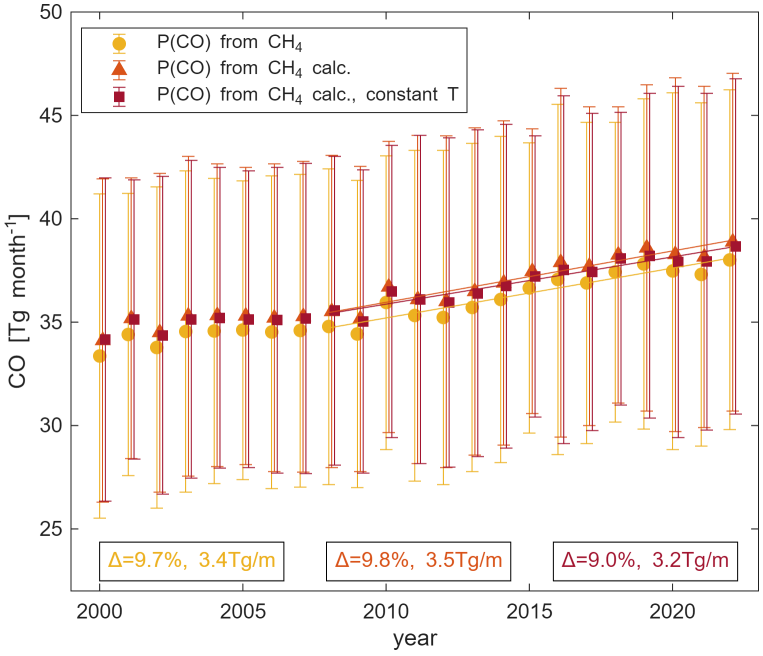

Figure S12. Changes of the CO production term from CH_4 and OH as GEOS-Chem ouput (yellow circles), calculated from GEOS-Chem outputs of CH_4, OH and k(CH_4+OH) (orange triangles) and calculated with constant temperature set to the values of 2011 (red squares).

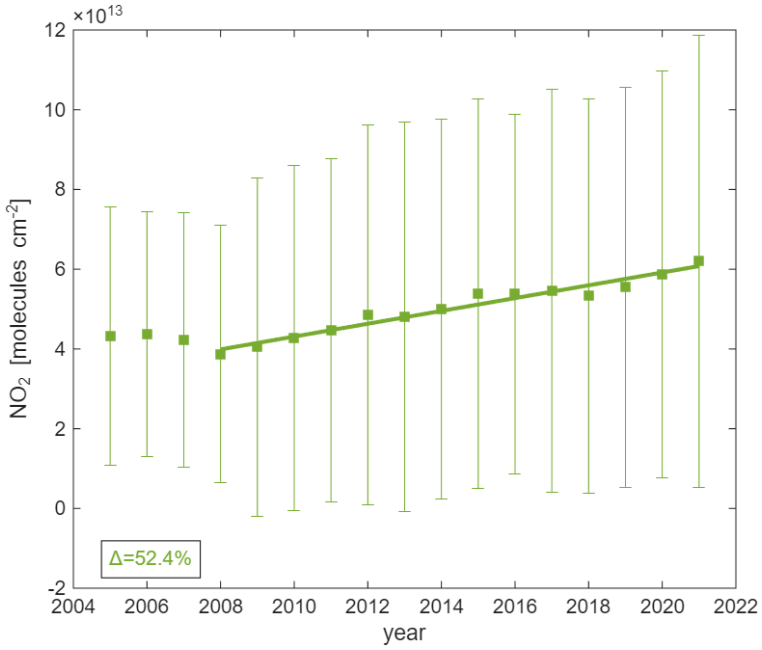

Figure S13. NO_2 column changes between 2005 and 2021 based on satellite retrievals from the OMI instrument South of 30°S. Symbols show yearly weighted averages (using the sample weight) and error bars represent the temporal uncertainty (1σ standard deviation of the temporal averaging). The solid line indicate the linear fit between 2008 and 2021 and the box shows the relative change of NO_2 over this time period. The trend is significant (p-value$<$0.05).